International Journal of Modern Physics B
Vol. 33, No. 0 (2019) 1950364 (9 pages)

DOI: 10.1142/S0217979219503648

Multi-band and broadband metamaterial perfect absorber based on conductive polymer and near-field coupling

Le Dac Tuyen[*,§,‖], Pham The Linh[†], Dang Hong Luu[†], Le Danh Phuong[†], Tong Ba Tuan[*], Tran Manh Cuong[‡] and Vu Dinh Lam[†,¶,‖]

[*] *Department of Physics, Hanoi University of Mining and Geology, 18 Pho Vien, Hanoi, Vietnam*

[†] *Graduate University of Science and Technology, Vietnam Academy of Science and Technology, 18 Hoang Quoc Viet, Hanoi, Vietnam*

[‡] *Faculty of Physics, Hanoi National University of Education, 136 Xuan Thuy, Hanoi, Vietnam*

[§] *ledactuyen@humg.edu.vn*

[¶] *lamvd@ims.vast.ac.vn*

Received 3 April 2019
Revised 22 October 2019
Accepted 22 October 2019
Published

We present a simple method for enhancing the bandwidth and absorptivity of metamaterial perfect absorber (MPA)-formed disk resonators. Utilizing low-conductivity polymer and near-field coupling of multi-band resonances, a 6.8 GHz broadband MPA is achieved with absorption over 90%. The proposed MPA also shows polarization-independent absorption behavior. Furthermore, the structural design is useful for making broadband MPA and can be applied to higher frequencies with a simple configuration.

Keywords: Metamaterials; perfect absorber; conductive polymer; near-field coupling.

AQ: Please provide PACS numbers

1. Introduction

Metamaterials (MMs) possess unique electromagnetic performance, which has a lot of practical applications such as invisible cloaking,[1] perfect lens,[2] sensor,[3,4] and energy harvesting.[5,6] Among them, metamaterial perfect absorber (MPA) has attracted attention due to its various advantages in thinness and tailoring frequency.[7,8] Since the pioneering MPA was developed by Landy *et al.* in 2008,[7] many MPAs have been demonstrated in different regions from microwave to optical frequency.[6–14] Most of the traditional MPAs in metal–insulator–metal configuration so far show a narrow absorption bandwidth, thus limiting their applications.

[‖] Corresponding authors.

To achieve broadband absorption MPA, great efforts have been proposed such as optimizing geometrical structure with multi-sized or multi-shaped resonators,[15–17] multiple metal–dielectric layers,[18–20] electronic devices[21] and plasmonic absorption.[13,16] However, the related processing techniques are more complicated and difficult to fabricate the sample. Especially, the fabrication techniques are still a great challenge for operating in the optical frequency. Therefore, the finding of an MPA structure that is simple and controllable to obtain broadband and high absorptivity is necessary. In a previous study, we have successfully fabricated a broadband MPA based on conductive polymer.[22]

In this work, we propose a simple and new approach to create multi-band and broadband MPA based on disk structure of a conductive polymer. Conceiving the MPA design involves the conductivity of the polymer to obtain higher absorptivity. By exploiting the near-field coupling of disk resonators, the broadband absorption can be generated. The proposed MPA has achieved absorption over 90% in the frequency range of 6.8 GHz. Furthermore, the absorption mechanism of the proposed MPA is analyzed by using the electric field distributions and impedance matching condition.

2. Structure and Design

Figure 1 illustrates the unit-cell design of the proposed MPA structure consisting of two layers of FR-4 dielectric substrate and copper film with periodicity $a =$ 20 mm. The FR-4 substrate has a dielectric constant of 4.0 and a loss tangent of 0.025. The copper film has an electric conductivity of 5.96×10^7 S/m. The thicknesses of dielectric FR-4 layer and copper film are $t_d = 1.6$ mm and $t_m =$ 0.036 mm, respectively. A patterned structure consists of four identical disks that are embedded in the FR-4 dielectric substrate. The disks are separated from each other with distance d, which have filled up with copper or a conductive polymer. The radius and depth of the patterned disks are $r = 2.4$ mm and $t_p = 0.036$ mm,

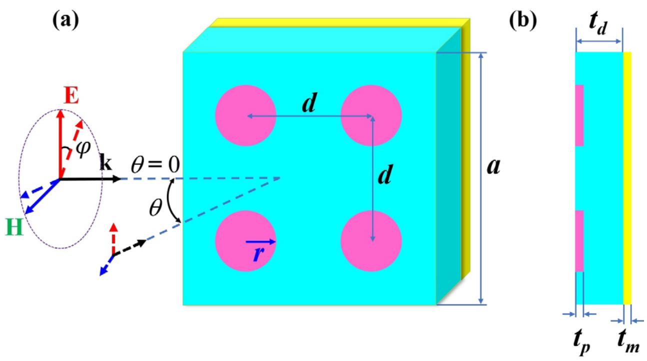

Fig. 1. (Color online) A schematic diagram of the unit cell of MPA with the electromagnetic wave: (a) 3-D view and (b) side view. $a = 20$ mm, $t_d = 1.6$ mm, $t_m = 0.036$ mm, $r = 2.4$ mm and $t_p = 0.036$ mm.

respectively. The electromagnetic (EM) wave with polarization angle φ and incident angle θ is shown in Fig. 1(a).

Numerical simulations are performed using CST Microwave Studio.[23] Due to the presence of the back layer as a copper film, the transmission $S_{21}(\omega)$ can be set to zero. Therefore, the absorption can be calculated as $A(\omega) = 1 - |S_{11}(\omega)|^2$, where $S_{11}(\omega)$ is the reflection parameters. Electric field distribution is also performed.

3. Result and Discussion

Figure 2 shows the absorption spectra of the copper disk and polymer disk MPAs with $d = 10$ mm. It is clearly observed that the absorption spectra consist of two resonance peaks, located at around 13.6 GHz (f_1) and 25.0 GHz (f_2). These two resonance peaks are slightly shifted to the lower frequency as the conductivity decreases. The absorptivity of the copper MPA is lower than that of polymer MPA. When the conductivity of the polymer is 100 S/m (solid line), the absorptivity of the polymer MPA increases up to 99% (f_1) and 95% (f_2), respectively. It indicates that the conductivity of polymer plays an important role to obtain higher absorptivity of MPA.

The absorption behavior can be explained by impedance matching condition.[24,25] Figure 3 shows the real part and imaginary part of the impedance for copper MPA and polymer MPA with the conductivity of 100 S/m, which are calculated by using S-parameters as

$$Z = \sqrt{\frac{(1+S_{11})^2 - S_{21}^2}{(1-S_{11})^2 - S_{21}^2}} = \frac{1+S_{11}}{1-S_{11}}. \tag{1}$$

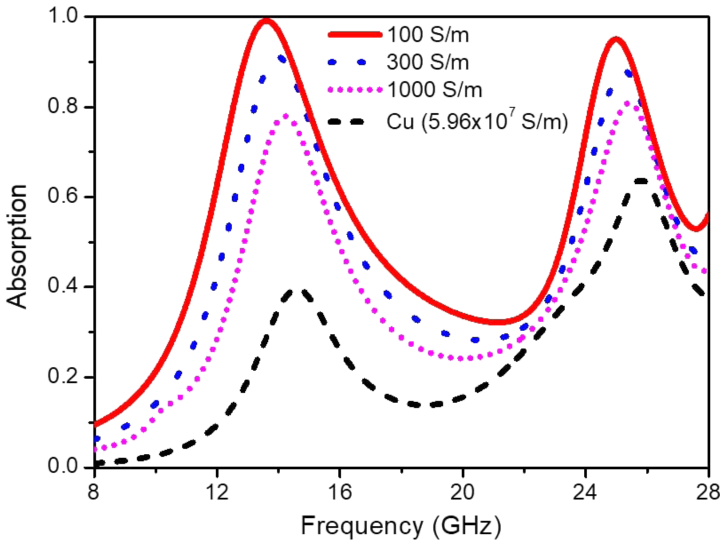

Fig. 2. (Color online) Simulated absorption spectra of the copper disk and polymer disk MPAs with different conductivity of the polymer. $a = 20$ mm, $t_d = 1.6$ mm, $t_m = 0.036$ mm, $r = 2.4$ mm, $t_p = 0.036$ mm and $d = 10$ mm.

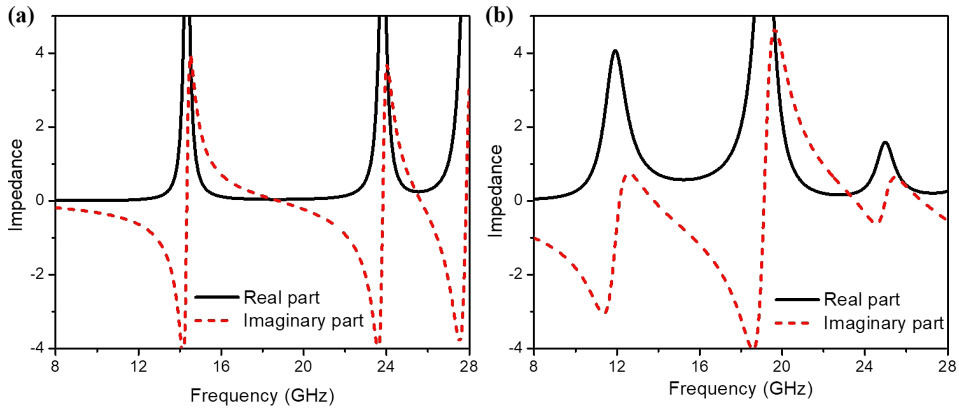

Fig. 3. (Color online) The impedance of the (a) copper MPA and (b) polymer MPA at normal incidence.

It indicates that the impedance of copper MPA is not well matched at both resonant frequencies [Fig. 3(a)]. However, in the case of the polymer MPA, the real part and imaginary part are approximately 1 and 0 at both resonances of 13.6 and 25.0 GHz, respectively [Fig. 3(b)]. Therefore, the impedance matching between the polymer MPA and free space has occurred, thus the near perfect absorption of the proposed

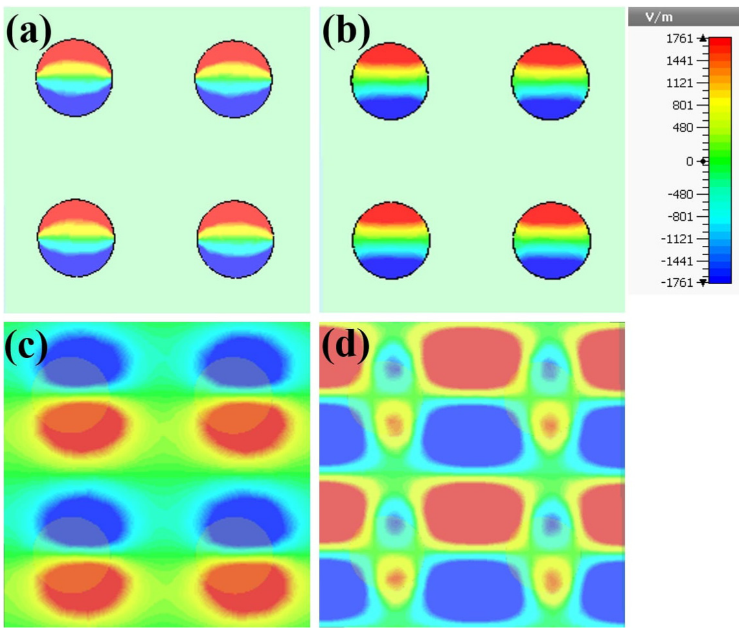

Fig. 4. (Color online) Electric field distributions on the (a, b) polymer disks and (c, d) back copper layer of the polymer MPA at (a, c) 13.6 GHz and (b, d) 25.0 GHz, respectively, when the conductivity of polymer is 100 S/m.

MPA is obtained.[24,25] As the results from Fig. 2, show the change of electrical conductivity induces the absorptivity is due to the changing effective impedance of MPA. It demonstrates that the electrical conductivity of the polymer affects the absorption behavior. The optimized value of electrical conductivity leads to the best impedance matching and high absorptivity.

To understand the absorption mechanism of the polymer MPA, we analyzed the electric field distribution at two resonant frequencies of 13.6 and 25.0 GHz as illustrated in Fig. 4. Overall, these two frequencies are both the electric dipole resonances excited on the polymer disks along the vertical direction [Figs. 4(a) and 4(b)]. However, the distribution on the copper film is significantly different. At the lower resonant frequency $f_1 = 13.6$ GHz, the electric field is locating at the polymer disk resonators [Fig. 4(c)]. However, the electric field is mainly concentrated on the space between horizontal disks at the higher resonant frequency $f_2 = 25.0$ GHz [Fig. 4(d)]. It indicates that the lower frequency is attributed to strong magnetic resonance.[15] While, at the higher frequency, the magnetic resonance is weak, and the near-field coupling resonance between adjacent disks induces absorption.[26,27]

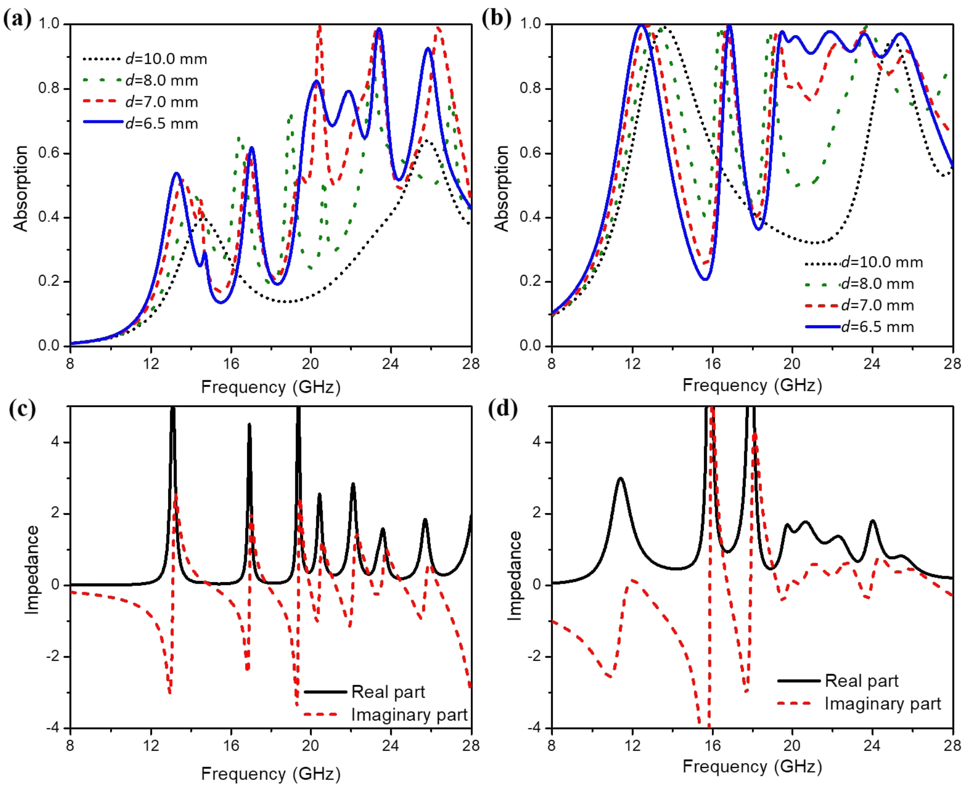

Fig. 5. (Color online) Influence of distance between adjacent disks d on the absorption spectra of the (a) copper MPA and (b) polymer MPA. The impedance of the (c) copper MPA and (d) polymer MPA with $d = 6.5$ mm.

In order to obtain broadband MPA, the distance between adjacent disks d is explored to evaluate absorption behavior. The position of the disks is changed along the diagonal of the unit-cell square. Figures 5(a) and 5(b) show the corresponding absorption spectra of the copper and polymer MPAs with different d.

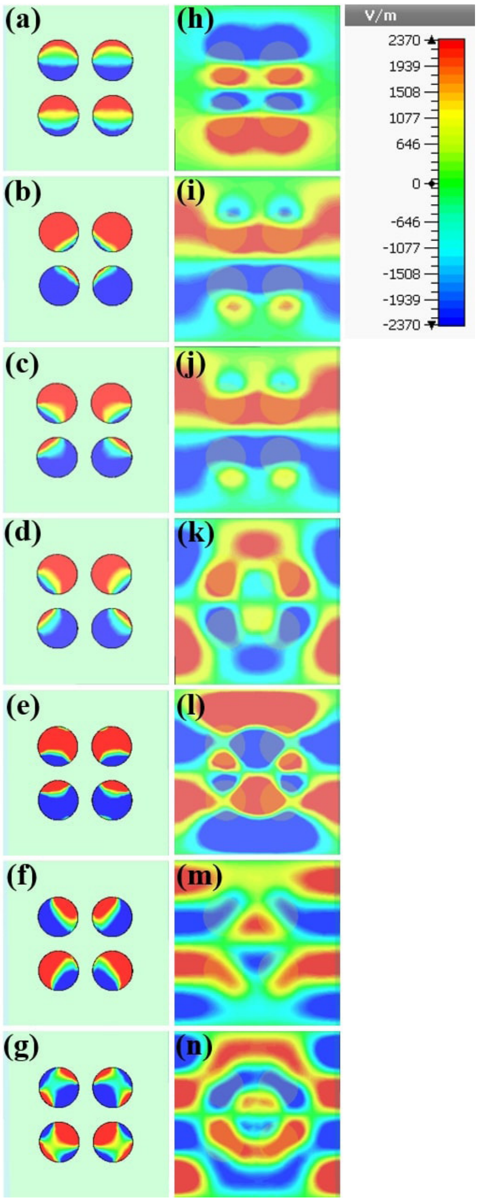

Fig. 6. (Color online) Electric field distributions on (a)–(g) the polymer disk with conductivity of 100 S/m and (h)–(n) back copper layer of the MPA at (a, h) 12.5 GHz, (b, i) 16.8 GHz, (c, j) 19.5 GHz, (d, k) 20.2 GHz, (e, l) 21.9 GHz, (f, m) 23.4 GHz and (g, n) 25.4 GHz, respectively.

For $d = 10.0$ mm, the disk position is center of each quadrant as discussed above. As d decreases from 10.0 to 6.5 mm, one can clearly observe seven prominent absorption peaks in both cases of the copper and polymer MPAs. For $d = 6.5$ mm, a combination of the third to seventh peaks of the polymer MPA broadens an absorption over 90% in the frequency range from 19.2 to 26.0 GHz, while the copper MPA is not. These can be explained by the impedance condition, as shown in Figs. 5(c) and 5(d). In the case of the polymer MPA, the real part and imaginary part are approximately 1 and 0 in the absorption frequency range, respectively [Fig. 5(d)], while the impedance of the copper MPA is not well matched [Fig. 5(c)].

In addition, Fig. 6(a)–6(n) show the electric field distribution on the polymer disks and back copper plane at the seven absorption peaks of 12.5, 16.8, 19.5, 20.2, 21.9, 23.4 and 25.4 GHz, respectively. The peaks at 12.5 GHz are fundamental magnetic resonances. However, at the higher frequency, other resonances are strong coupling between adjacent disks, resulting in broadband absorption of multi-resonance peaks. It indicates that the electric conductivity of polymer and near-field coupling can significantly enhance the bandwidth and absorptivity of MPA.

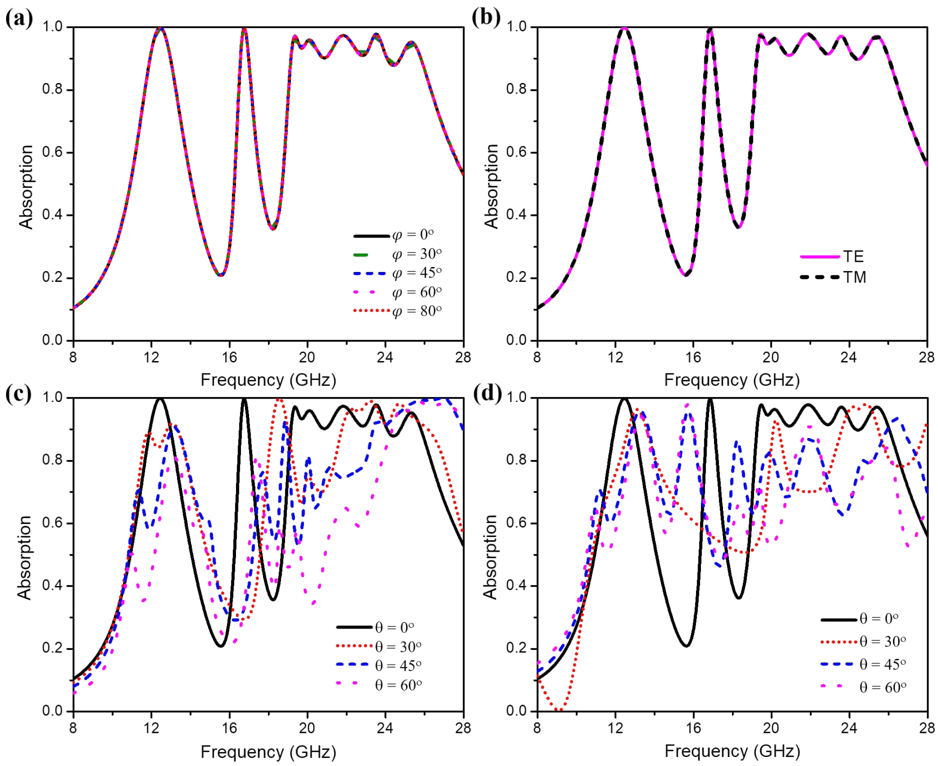

Fig. 7. (Color online) (a) Dependence of absorption spectra on the polarization angle φ for TE mode at normal incidence. (b) Comparison of absorption spectra for TE and TM modes at normal incidence. Dependence of absorption spectra on the incident angles for (c) TE and (d) TM polarizations.

To evaluate the absorption behavior of proposed MPA, the dependence of absorption spectra on the different polarization under both transverse electric (TE) and transverse magnetic (TM) polarizations are investigated. Figure 7(a) presents the absorption spectra at normal incidence for TE polarization with different polarization angles φ from 0^o to 80^o. Similarly, the absorption spectra at normal incidence for TM polarization in the same TE polarization are shown in Fig. 7(b). It is not surprising that the polymer MPA shows polarization insensitivity due to its symmetry of structural design.

Furthermore, the dependence of absorption spectra on the incident angles for both TE and TM polarizations is present in Figs. 7(c) and 7(d), respectively. The polymer MPA exhibits a blue-shift of the multi-resonance peaks and displays other absorption dips from 19 to 24 GHz when the incident angle increases, resulting in lower absorption efficiency and narrower bandwidth. It indicates the near-field coupling between adjacent disks is strongly dependent on the incident angle.

AQ: Please approve edit.

4. Conclusion

We have proposed a broadband and polarization-independence MPA based on conductive polymer material with a simple configuration. Due to the low conductivity of polymer, absorption is exceeding 90% with wide bandwidth from 19.2 to 26.0 GHz by near-field coupling resonances. The structural design can be applied to higher frequencies and is useful for making broadband MPA with a simple configuration.

Acknowledgments

This research is funded by Vietnam National Foundation for Science and Technology Development (NAFOSTED) under grant number 103.02-2017.67.

References

1. J. B. Pendry, D. Schurig and D. R. Smith, *Science* **312**, 1780 (2006).
2. J. B. Pendry, *Phys. Rev. Lett.* **85**, 3966 (2000).
3. T. S. Bui *et al.*, *Sci. Rep.* **6**, 32123 (2016).
4. B. S. Tung *et al.*, *Mod. Phys. Lett. B* **32**, 1850044 (2018).
5. M. K. Hedayati *et al.*, *Adv. Mater.* **23**, 5410 (2011).
6. M. Bagmanci *et al.*, *Int. J. Mod. Phys. B* **33**, 1950056 (2019).
7. N. I. Landy *et al.*, *Phys. Rev. Lett.* **100**, 207402 (2008).
8. B. X. Khuyen *et al.*, *Curr. Appl. Phys.* **16**, 1009 (2016).
9. Y. J. Kim *et al.*, *Curr. Appl. Phys.* **17**, 1260 (2017).
10. M. Tonouchi, *Nat. Photon.* **1**, 97 (2007).
11. D. Hu *et al.*, *J. Nonlinear Opt. Phys. Mater.* **25**, 1650032 (2016).
12. R. Bai *et al.*, *J. Nonlinear Opt. Phys. Mater.* **25**, 1650027 (2016).
13. W. Wang *et al.*, *Appl. Phys. Lett.* **110**, 101101 (2017).
14. F. Ding *et al.*, *Sci. Rep.* **6**, 39445 (2016).
15. D. T. Viet *et al.*, *Opt. Commun.* **322**, 209 (2014).
16. K. Aydin *et al.*, *Nat. Commun.* **2**, 517 (2011).

AQ: Please provide year.

17. Y. Cui *et al.*, *Appl. Phys. Lett.* **99**, 253101 (2011).
18. Y. Cui *et al.*, *Nano Lett.* **12**, 1443 (2012).
19. N. T. Tung *et al.*, *J. Nonlinear Opt. Phys. Mater.* **18**, 489 (2009).
20. Y. J. Kim *et al.*, *Opt. Express* **23**, 3861 (2015).
21. D. Lee, H. Jeong and S. Lim, *Sci. Rep.* **7**, 4891 (2017).
22. L. D. Hai *et al.*, *Opt. Express* **26**, 33253 (2018).
23. *CST Microwave Studio: A Numerical Simulation Software for Electromagnetic Computing* (Computer Simulation Technology GmbH, Darmstadt, Germany), https://www.cst.com.
24. D. R. Smith *et al.*, *Phys. Rev. E* **71**, 036617 (2005).
25. H. T. Chen, *Opt. Express* **20**, 7165 (2012).
26. H. L. Dang *et al.*, *J. Nonlinear Opt. Phys. Mater.* **26**, 1750036 (2017).
27. B. S. Tung *et al.*, *Sci. Rep.* **7**, 11507 (2017).